RESEARCH

Pore structure response at different scales in coal to cyclical liquid nitrogen treatment and its impact on permeability and micromechanical properties

Changbao Jiang · Qi Sun · Bozhi Deng · Bowen Yang · Jianquan Guo

Abstract The methane in the coal seams of abandoned mines is a valuable natural gas resource. However, the ultra-low permeability of coal seams restricts the extraction of coalbed methane. The liquid nitrogen fracturing technology is a novel approach suitable for enhancing the permeability of coal seams in abandoned mines. The ultra-low temperature could potentially facilitate the growth and propagation of pores and fractures in coal seams. In this study, we observed inconsistent alterations in coal properties measured by multiple instruments at different scales, whether in dry or wet coal specimens. This suggests that the mechanisms influencing the pore structure due to LN_2 treatment differ across various scales in dry and wet coal specimens. For dry specimens, heterogeneous thermal deformation and freezing shrinkage exhibited opposing effects during LN_2 treatment. Thermal stress-induced micro-fractures might counteract the freezing contraction of micropores in coal matrices, preventing a significant decrease in coal macropores and fractures. In wet specimens, the effects of LN_2 treatment on wet coal specimens were predominantly controlled by frost heaving. However, due to low water saturation, LN_2 treatment had negligible effects on coal micropores, even in the presence of local frost heaving. In field applications, water migration from smaller to larger pores could further diminish the impact of LN_2 treatment on micropores.

Article highlights

- LN_2 treatment has different effects on the change in pore structure of coal at multi-scale.
- The thermal stress-induced fractures and micropores contraction occur in coal matrices.
- Water migration may further reduce the effects of LN_2 treatment on the micropores of coal.

1 Introduction

With the long-term exploitation of China's coal resources, more and more production mines are being scrapped due to resource depletion. And in the context of carbon neutral and national new energy strategy, China is expected to close/abandon 15,000 coal mines in 2030 due to capacity removal and energy

C. Jiang · Qi. Sun · B. Deng (✉) · B. Yang
State Key Laboratory of Coal Mine Disaster Dynamics and Control, School of Resources and Safety Engineering, Chongqing University, Chongqing 400030, China
e-mail: Dengbz@cqu.edu.cn

J. Guo
Jining No.3 Mine, Yankuang Energy Group Co., Ltd., Jining 272169, China

structure adjustment (Ping et al. 2020; Yuan et al. 2018). These abandoned mines are rich in abandoned mine methane resources (Cheng et al. 2023; Feng et al. 2018; Li et al. 2021). Abandoned mine methane as a usable resource and the possible harm to the environment cannot be ignored, so the extraction of abandoned mine methane has become one of the important resources for coalbed methane in coal mining areas (Xie et al. 2017).

Coalbed methane (CBM) extraction technology is hydraulic fracturing (Zoback et al. 1977; Li et al. 2022; Zhang et al. 2022; Khadijeh et al. 2022), this technique employs high-pressure water flow as a power carrier to pressurize boreholes and impart tensile stress to the rock masses, causing them to fracture. Water eventually fractures the rock mass and forces fractures to propagate away from the boreholes, which can significantly enhance the permeability of the target reservoirs. However, in the process of fracturing, a large amount of water will pour into the coal reservoir, which is fatal for abandoned mines. After the closure of the coal mine, the drainage of the mine pit stops, and the water level in the mine rebounds and rises. The mine water seeps out through coal seams and tunnel cracks, carrying a large number of harmful substances into the groundwater, causing serious water resource problems such as groundwater and surface water pollution (Wolkersdorfer et al. 2022; Liu et al. 2022). Therefore, hydraulic fracturing technology is clearly no longer suitable for gas extraction in abandoned mines. The new permeability enhancement technology not only needs to improve the recovery rate of fractured coal seams, but also needs to prevent mine water from flowing out of abandoned mines with newly added cracks, causing serious environmental pollution problems.

The first application of liquid nitrogen freezing in geological engineering can be traced back to 1979 (Stoss and Valk 1979). Since then, it has been widely used for temporary foundations, large open excavation, and soil deposits. Artificial ground freezing methods can enhance the mechanical properties or decrease the hydraulic conductivity of soil (Won et al. 2022). Later studies indicated that the temperature effect of freeze–thaw cycles can induce the breakage of hard rock, which may be beneficial or harmful for different geologic engineering projects, such as tunnel excavation or the disposal of deeply buried nuclear waste (Hou et al. 2021; Momeni et al. 2016).

The injection of LN_2 into a geologic formation and its vaporization will cause the geological mass to go through a freeze–thaw cycle (Sun et al. 2023). Therefore, applying LN_2 for rock fracturing has attracted attention from unconventional geo-energy fields such as geothermal energy, shale gas, and coalbed methane. Compared with hydraulic fracturing, LN_2 fracturing has the advantages of low-off rate, low reservoir damage and no sewage during fracturing processes (Zhang and Hascakir 2021), which may be more suitable for upgrading coal seam permeability in abandoned mines. Firstly, the low temperature environment caused by liquid nitrogen injection can generate thermal stress to fracture the coal and enhance the permeability of the coal seam, and secondly, the low temperature environment will freeze the original water in the coal seam into ice, which can not only generate freezing expansion force to further expand the fracture, but also control the water migration and inhibit the seepage of mine water. After fracturing, gaseous nitrogen can reduce the partial pressure of methane and promote desorption (Ottiger et al. 2008).

Many studies have focused on the variation in the mechanical properties, pore structure, and fracture systems of coal induced by LN_2 treatment. Cai et al. (2015; 2016) performed laboratory experiments based on traditional rock mechanical experiments to investigate the evolution of the mechanical properties of coal following LN_2 treatment. It was determined that the change in the pore and fracture structures resulted in the deterioration of the coal. Su et al. (2020) conducted Brazilian split experiments on LN_2-treated coal samples. The variation in tensile strength, crack surface, and microscopic structures indicated that the bedding structure and pre-existing fractures were more vulnerable during the LN_2 treatment. Yin et al. (2018) and Cai et al. (2014) measured the permeability of coal before and after the LN_2 treatment and compared the cracks on the surface of a coal sample. It was observed that the increase in coal permeability was closely related to meso- and macroporosity and fractures. Zhao et al. studied the effects of freeze–thaw cycles and water saturation on the results of LN_2 treatment. The increase in the number of freeze–thaw cycles and water saturation can significantly enhance the variation in the pore structure of coal. Zhai et al. (2016) and Qin et al. (2016; 2017; 2019; 2022) comprehensively studied the pore characteristics

of the coal samples before and after LN$_2$ treatment using nuclear magnetic resonance technology. They determined that the cyclic LN$_2$ treatment can induce larger pores as flow channels and increase the permeability of coal. Additionally, the experimental results indicated that the properties of lignite change more and that the greater the moisture content, the greater the damage. Han et al. (2018) reported that fractures on the shale surface gradually increased with an increase in the number of LN$_2$ treatment cycles. A connected fracture network was formed after the fourth LN$_2$ treatment cycle, implying that the freezing and thawing processes have a significant effect on the evolution of the fracture and pore structure of rocks.

The effects of LN$_2$ treatment on rocks were mainly attributed to thermal stress, which is induced by heterogeneous thermal expansion (Jiang et al. 2021; Wang et al. 2020). However, in the presence of mine water, a frost heaving force can be induced to cause more damage to rocks. It is difficult to distinguish the effects of thermal stress and frost heaving force on the mechanical properties and pore structures of coal. Traditional rock mechanical tests and porosity and permeability measurements primarily reflect the macroscopical variation of coal. The microscopical variation in the pore structure and mechanical properties of coal were barely investigated. In particular, water migration in multi-scale pores during the freeze–thaw cycles and its effects on the coal matrix and fracture system remain unknown.

Therefore, in this study, the variation in mechanical properties and pore structures of dry and wet coal specimens in response to cyclic LN$_2$ treatment was investigated by different testing instruments at multiscales, such as permeability measurement, NMR, and nano-indentation. The connections between the experimental results obtained through different measurement methods were carefully analyzed. The presence of water and its migration among the coal pores at the different scales were comprehensively studied by comparing the difference between the dry and wet coal specimens. The effects of thermal stress and frost heave force on the coal matrix and fracture system were discussed separately. The contribution of this work may deepen the understanding of liquid nitrogen treatment mechanism and its on-site application in abandoned mines.

2 Experiment

2.1 Specimen preparation

The coal specimens used in this study were obtained from the province of Guizhou, China. Table 1 lists the proximate analysis parameters for the coal specimens. Coal blocks were first collected from a coal mine in Bijie City. Then, the same coal block was cut into two types of shapes. The first type is cylindrical coal specimens (100 mm in height and 50 mm in diameter), which were prepared for permeability and nuclear magnetic resonance tests. The second type is small coal disks (5 mm in height and 10 mm in diameter), which were prepared for nano-indentation experiments. The coal specimens used in the experiments are illustrated in Fig. 1. Twenty-four cylindrical specimens were divided into dry and wet groups. First, all the coal specimens were oven-dried for 24 h. Then, 12 specimens, which were marked as dry specimens preparing for LN$_2$ treatment, were taken out. Other specimens were placed in a vacuum device for 24 h to achieve water saturation. Finally, the water-saturated specimens were taken out and marked as wet specimens. The water content was measured by the weight of the coal specimens before and after the water saturation. The wet coal disks were water saturated using the same procedure.

2.2 Experimental apparatus

A liquid nitrogen tank was prepared for the LN$_2$ treatment. In addition to the LN$_2$ treatment device, a series of other devices were used to determine the variation in mechanical properties and pore structures of dry and wet specimens at different scales. The variation of coal fractures from µm to mm in response to the LN$_2$ treatment was reflected in the permeability measurements. Nano-indentation demonstrated the variation in mechanical properties of coal from the

Table 1 Proximate analysis parameters of coal specimens

Rank	Proximate analysis parameters (mass percentage, %)			
	Moisture	Ash	Volatile	Fixed carbon
Anthracite	2.41	21.90	7.60	68.09

Fig. 1 Photographs of the coal specimens used in this study: **a** cylindrical coal specimens for NMR experiments and permeability measurements; **b** disk coal specimens for SEM observations and nano-indentation experiments


(a)   (b)
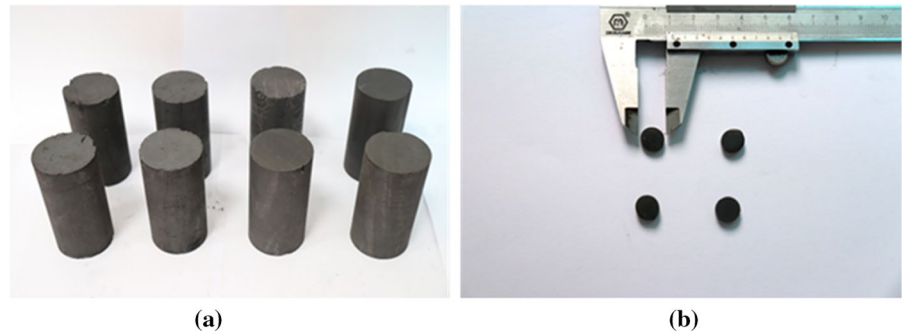
nm to the μm scale. NMR pore analysis revealed the variation in full pore size distribution from the nm to the mm scale. Therefore, the effects of LN_2 treatment on dry and wet specimens can be comprehensively investigated through the series of experiments. The experimental results obtained by different devices at the same scale showed good agreement.

Figure 2 shows the images of the series of experimental devices that were used. To investigate the permeability change of LN_2-treated coal, a conventional triaxial servo-controlled (CTS) apparatus, developed by the State Key Laboratory of Coal Mine Disaster Dynamics and Control at Chongqing University, was employed. The minimum flow rate measurement accuracy was 0.001 L/min. Furthermore, to investigate the pore structure variation of LN_2-treated coal, a nuclear magnetic resonance instrument developed by Newmai Electronic Technology LLC was employed. For the experimental specimens, the shortest echo time recorded was less than 200 s. A TI 950 TriboIndenter nanoindenter developed by Hysitron Company was employed to investigate the damage to the mechanical properties of LN_2-treated coal. The measurement sensitivities were < 30 nN and < 0.2 nm. A Phenom Pro Desktop scanning electronic microscope was employed to observe the fracture propagation on the LN_2-treated coal surface. The resolution was set to 6 nm.

The nano-indentation device was utilized to measure the mechanical properties of coal specimens on a scale ranging from nm to mm. Figure 3 illustrates the principle of indentation and depicts the obtained experimental curve. Based on the classic Oliver–Pharr method, the maximum displacement, maximum loading, and slope of the unloading curve illustrated were extracted from the loading–displacement curve as h_{max}, F_{max}, and contact stiffness $S = dF/dh$, respectively. According to the morphology of a Berkovich indenter, the contact area A_c can be calculated using Eqs. (1) and (2).

Fig. 2 Photographs of the experimental apparatus employed in this study: **a** coal permeability measurement equipment, **b** nano-indentation equipment, **c** NMR equipment for pore structure measurement, and **d** SEM system
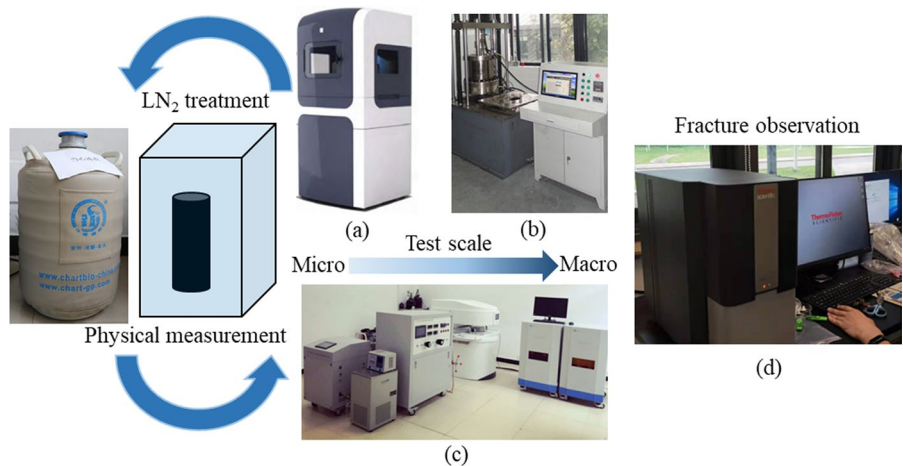
Fig. 3 Indentation experiments. **a** Sketch of indentation experiments; **b** a typical curve of a nano-indentation experiment and key parameters required for mechanical calculation

(a)   (b)
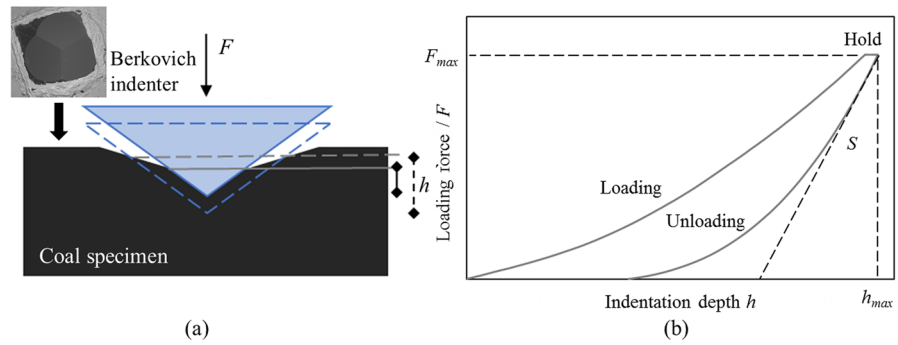
$$h_c = h_{\max} - 0.75 \times \frac{F_{\max}}{S} \tag{1}$$

$$A_c = 3\sqrt{3}hc^2 \tan^2 65.3° = 24.56hc^2 \tag{2}$$

where h_c is the contact depth. Based on contact mechanics, the reduced modulus E_r can be calculated using Eq. (3).

$$E_r = \frac{\sqrt{\pi}}{2\beta\sqrt{A_c}}S \tag{3}$$

where $\beta = 1.034$ for the Berkovich indenter. The reduced modulus represents the uniform modulus of the indenter and tested material. Thus, the relationship between the reduced modulus and elastic modulus of the indenter and the tested material can be expressed by Eq. (4).

$$\frac{1}{E_r} = \frac{1-v^2}{E} + \frac{1-v_i^2}{E_i} \tag{4}$$

where $E_i = 1141$ GPa and $v_i = 0.07$ represent the elastic modulus and Poisson's ratio of the indenter, respectively; E and v represent the elastic modulus and Poisson's ratio of the tested material, respectively.

Moreover, indentation hardness H can be calculated using Eq. (5).

$$H = \frac{F_{\max}}{A(h_c)} \tag{5}$$

The permeabilities of the cylindrical coal specimens, which reflected the variation in seepage pores of coal specimens, were measured using the steady flow method. The inlet pressure P_1, outlet pressure P_2,

and flow rate at the outlet were recorded for the permeability calculation using Eq. (6).

$$k = \frac{2\mu QPL}{A\left(P_1^2 - P_2^2\right)} \tag{6}$$

where k represents the permeability (m^2), P represents standard atmospheric pressure (Pa), μ represents the dynamic viscosity of gaseous nitrogen, which is 17.80 μPa·s, Q represents flow rate (L/min), A represents the basal area of the coal specimen (m^2), and L represents the length of the coal specimen (m).

The full pore size distribution was measured using NMR. It reflects the relaxation characteristics of the hydrogen containing fluids in rock pores based on the interaction principle between the magnetism of the hydrogen atomic nucleus and the external magnetic field. The number of hydrogen atoms in the fluid in the pores and fractures of coal after saturation is determined by the transverse relaxation time T2. The characteristics of the pores and fracutres of coal can be analyzed through relaxation time T2. The relationship between the transverse relaxation time T2 and the pore diameter of coal can be expressed by the following formula:

$$\frac{1}{T_2} = \rho_2\left(\frac{S}{V}\right) = F_S\frac{\rho_2}{r} \tag{7}$$

$$r = cT_2 \tag{8}$$

where S is the surface area of pores, V is the volume of pores, ρ_2 is the transverse surface relaxation strength of rock (which is a constant), F_s is the geometric shape factor ($F_s = 3$ for spherical pores and $F_s = 2$ for cylindrical pipes), c is the conversion coefficient (m/s), and r is the hole diameter.

The T2 spectrum can provide a clear and intuitive quantification of the pore structure in coal. The distribution of relaxation time T2 can reflect the change in pore diameter. The total area of the T2 distribution spectrum represents the total pore volume of coal. Through mathematical calculation, the signal amplitude can be converted into porosity. The total porosity of the coal body can be obtained by accumulating the porosity components over time.

2.3 Experimental scheme

The LN_2 treatment used in this study followed the following procedure. First, the prepared coal specimens were subjected to a series of experiments to measure the physical properties of coal specimens in their original condition. Then, they were wrapped in plastic to prevent LN_2 and air moisture intrusion. Subsequently, the treated coal specimens were removed and placed in a liquid nitrogen tank for 30 min to completely freeze the water in the micro and macropores. Finally, the wrapped coal specimens were placed in a container to gradually increase their temperature. The aforementioned procedure was regarded as a single LN_2 treatment cycle. After different LN_2 treatment cycles, different physical properties (pore structure, permeability, and mechanical properties) of the treated coal specimens were measured for different experimental objectives.

Twenty-four cylindrical coal specimens were marked as D-N1-1, 2, 3, 4, 5, D-N7-1, 2, 3, 4, 5, W-N1-1, 2, 3, 4, 5, W-N3-1, W-N5-1, W-N7-1, 2, 3,4 5, W-P7-1, 2 (the letters D and W represent the dry and wet specimens, respectively; the letters N and P represent the NMR and permeability experiments, respectively. The number after N/P represents number of cycles of LN_2 treatment, and the last number represents the repeated experiment number). Two disk coal specimens were marked as W-I7-1 and W-S7-1 (I and S represent nano-indentation experiments and SEM observation, respectively). The experimental scheme is summarized in Table 2.

The identical regions and microfractures before and after coal impact cycling were compared through SEM observation. Additionally, nano-indentation experiments were performed in the same areas. The maximum value was set to 8 mN. In the permeability experiments, the confining pressure and axial stress were set to 2 MPa to avoid loading effects on the pore structure of the coal specimens. The inlet pressure for 99.99% nitrogen was set to 1 MPa.

3 Experimental results and analysis

3.1 Variation of mechanical properties at the microscale

Figure 4 illustrates the loading–displacement curves of the indentation experiments on W-I7-1, 2, 3, 4, and 5 at 0, 1, 3, 5, and 7 LN_2 treatment cycles. The gray dashed lines in Fig. 4 present the indentation depth equals to 1100 nm which can help me to distinguish the parallel translation of the indentation curves. It can be observed that the maximum indentation displacements of the disk coal specimen under an untreated condition are approximately 1100 nm. After seven LN_2 treatment cycles, all the maximum

Table 2 Experimental scheme

Coal specimen	Cycle number	Measure type of physical properties	Water content condition
D-N1-1, 2, 3, 4, 5	1	Pore structure (NMR)	Dry
D-N7-1, 2, 3, 4, 5	7	Pore structure (NMR)	Dry
W-N1-1, 2, 3, 4, 5	1	Pore structure (NMR)	Wet
W-N3-1	3	Pore structure (NMR)	Wet
W-N5-1	5	Pore structure (NMR)	Wet
W-N7-1, 2, 3, 4, 5	7	Pore structure (NMR)	Wet
W-P7-1, 2	7	Permeability (steady flow method)	Wet
W-I7-1, 2, 3, 4, 5	0, 1, 3, 5 and 7	Mechanical properties (nano-indentation)	Wet
W-S7	7	Microfracture propagation (SEM)	Wet
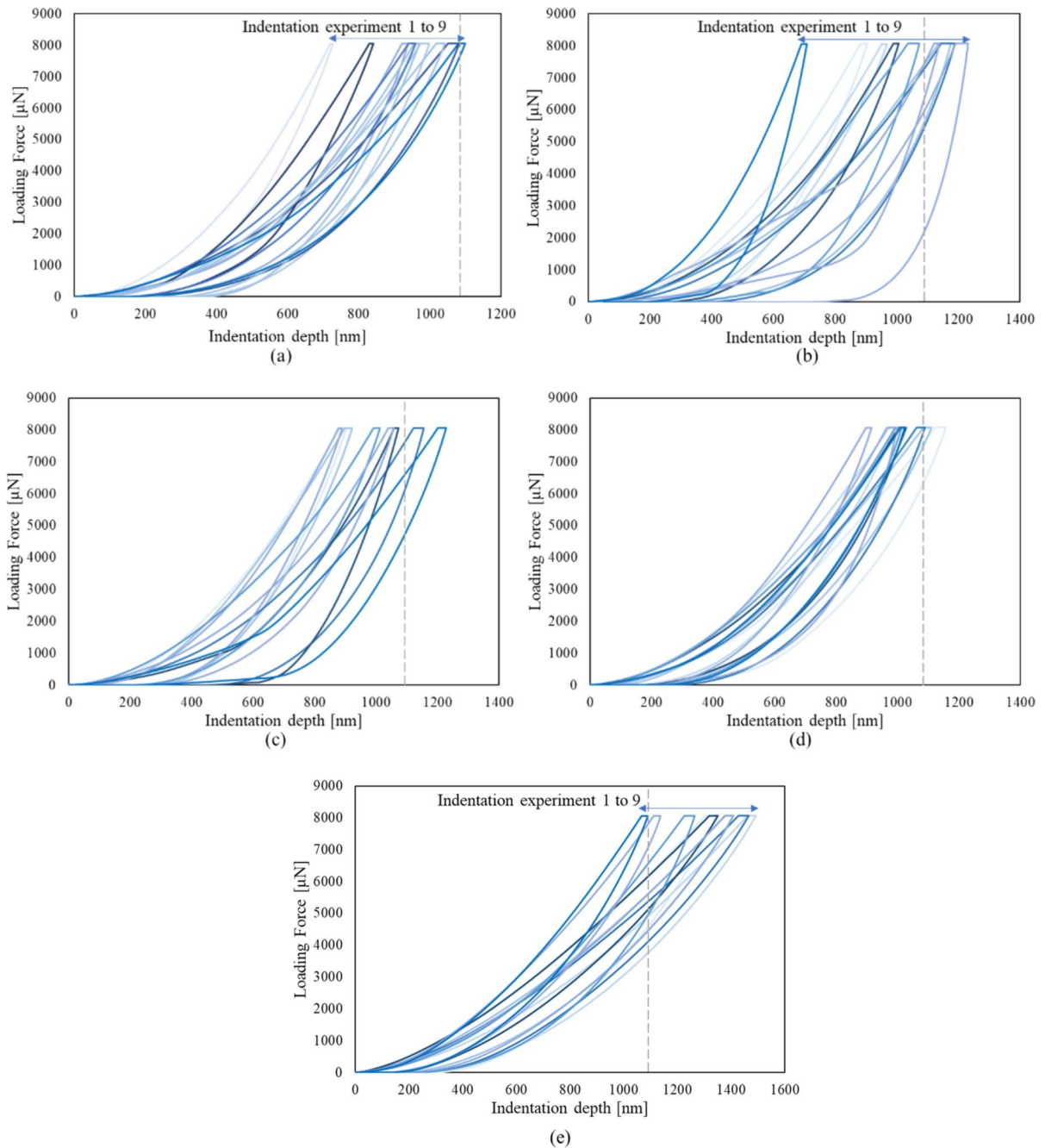
Fig. 4 Nano-indentation curves of wet coal specimens after different coal impact cycles (gray dashed line represents a depth = 1100 nm): **a** without cyclic LN$_2$ treatment, **b** after one cycle, **c** after three cycles, **d** after five cycles, and **e** after seven cycles

indentation displacements of the disk coal specimens were 1100 nm. However, there was no significant difference in the curves until the seventh cycle of LN$_2$ treatment. In the next steps, the indentation hardness and elastic modulus were calculated to quantitatively characterize the variation in the mechanical properties of coal at the microscale after cyclic LN$_2$ treatment.

Based on the analysis method presented in Sect. 2.2, the hardness and elastic modulus can be calculated through Eqs. (2) and (3). The whisker plot in Fig. 5 illustrates the calculated hardness and elastic modulus values. It can be observed that there is an outlier in the results of the untreated coal specimen. We considered this to be an indentation experiment on a hard mineral. The average and median values of the elastic modulus and hardness of the disk coal specimen within the five LN_2 treatment cycles were close to each other, indicating that the LN_2 treatment barely affected the mechanical properties of the coal matrix at the microscale. However, after the seventh coal impact cycle, the elastic modulus and hardness of the disk-shaped coal specimens decreased significantly. This could be attributed to the fact that the accumulation of changes in the pore structure reached a threshold, which damaged the coal matrix. Moreover, in Fig. 5a and b, the thickness of the boxes could be observed to decrease gradually with the increase in the LN_2 treatment cycles. This implies that the microstructure of the coal changed toward homogeneity during the LN_2 treatment.

3.2 Evolution of coal permeability

Figure 6 illustrates the permeability evolution of the coal specimens at different LN_2 treatment cycles.
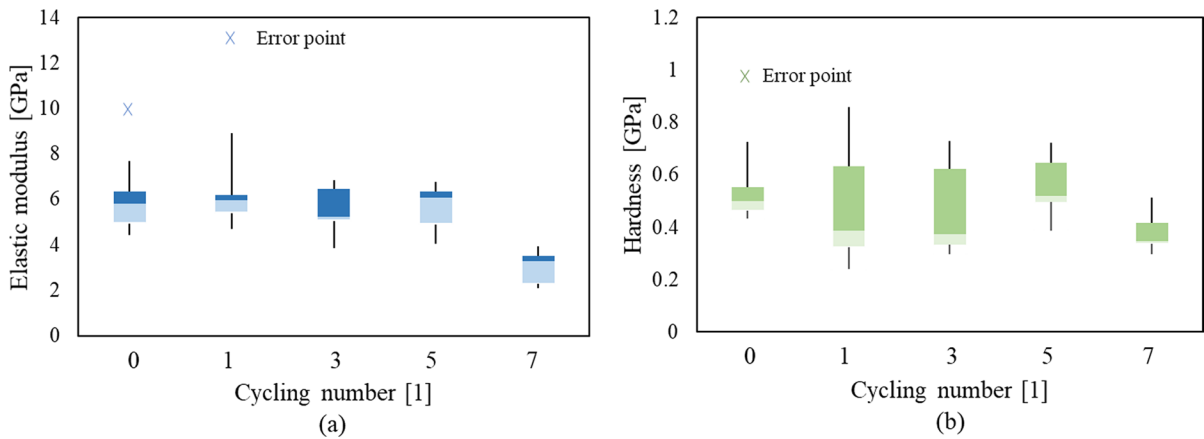
Fig. 5 Whisker plot of the calculated hardness and elastic modulus for nano-indentation experiments under different LN_2 treatment cycles. **a** calculated elastic modulus; **b** calculated hardness
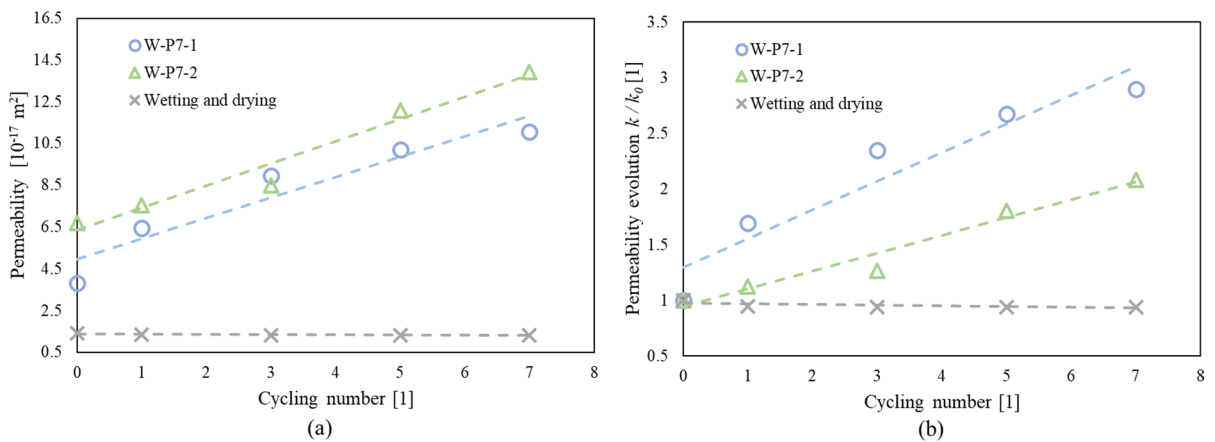
Fig. 6 Permeability evolution of coal specimens under different LN_2 treatment cycles: **a** absolute evolution and **b** relative evolution

Owing to the moisture loss in the permeability measurement, coal specimens should be placed in a water container to maintain a water saturation of 80% before every LN_2 treatment. Thus, the coal specimens underwent a wetting and drying process. This may have affected the permeability of the coal specimens. We conducted a contrast experiment to reveal the effects of wetting and drying cycles on coal permeability. Figure 6 illustrates the permeability evolution of the coal specimens for the wetting and drying experiments. It can be observed that, after cyclic LN_2 treatment, the permeability of coal specimens gradually increased from 3.814×10^{-17} to 1.105×10^{-16} m^2 for W-P1-7 and from 6.693×10^{-17} to 1.393×10^{-16} m^2 for W-P2-7. The extent of the increase in permeability was 189.90% and 151.16% for W-P1-7 and W-P2-7, respectively. The effects of wetting and

drying cycling were negligible, except for the first cycle (gray line). The increase in permeability could be fully attributed to LN_2 treatment. This phenomenon implies that the LN_2 treatment could enhance the flow channels, which are primarily microfractures and macropores in coal.

3.3 Variation of pore structure in coal

Figure 7 illustrates the T2 relaxation curves of the NMR experiments. Before comparing the T2 relaxation curves under different LN_2 treatment conditions, the relationship between pore types and T2 relaxation time was defined. The classification of pore types according to T2 relaxation time was based on a previous study (Li et al. 2017). The T2 relaxation times below 10 ms, between 10 and 100 ms, and
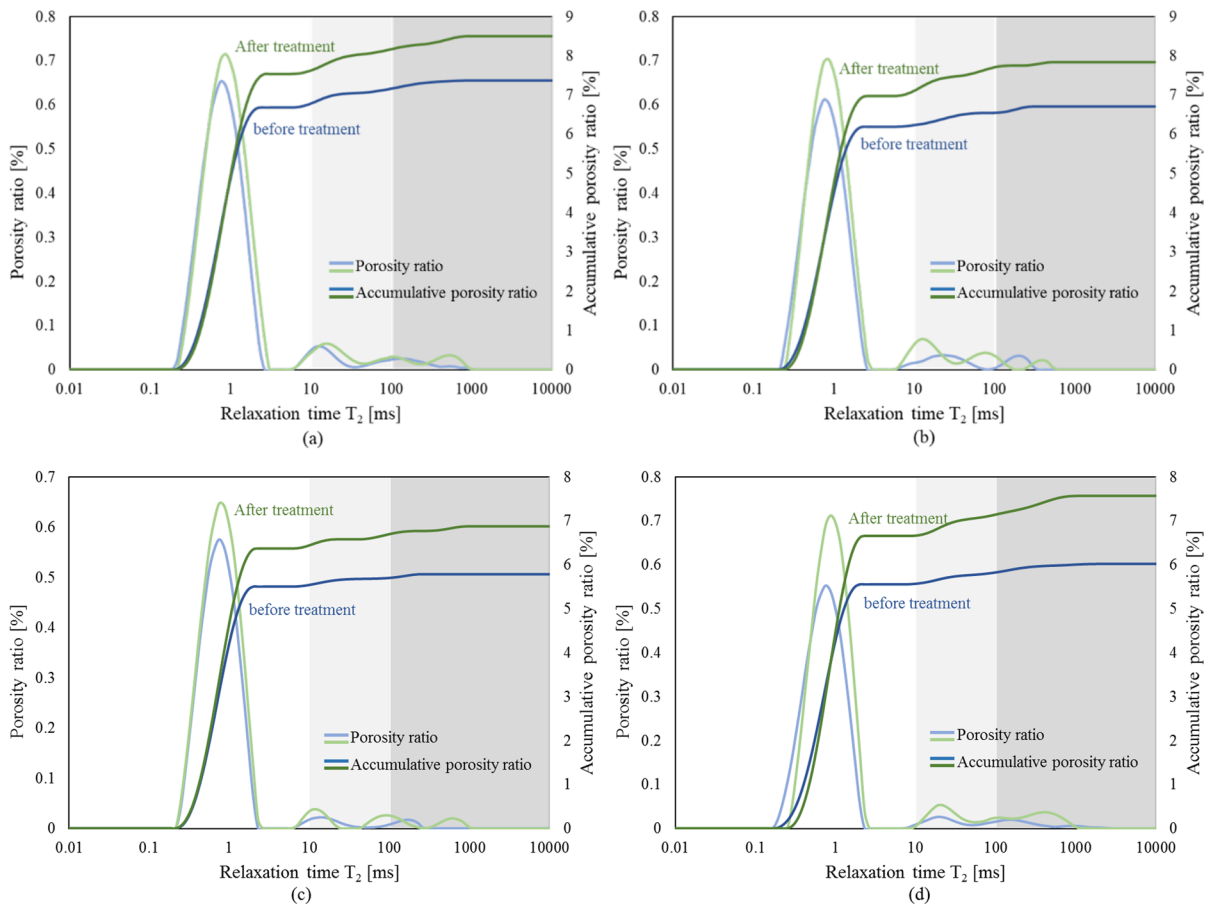
Fig. 7 T2 relaxation curves of NMR experiments for different coal specimens under different LN_2 treatment conditions: **a–d** wet coal specimens under 1–7 LN_2 treatment cycles; **e** and **f** dry coal specimens under 1–7 LN_2 treatment cycles

above 100 ms were identified as microporosity, mesoporosity, and macroporosity, respectively. Thus, the pore size distribution can be determined from the T_2 relaxation curves. The pore size distributions of all coal specimens could be observed to be very similar to each other. They all revealed that the microporosity developed the most, followed by the mesoporosity, which developed less, and the macroporosity, which showed the least development. The similar initial pore size distribution among the experimental coal specimens also verified the credibility of our subsequent analysis, which involved comparing the variations in the pore structure of different coal specimens.

The scope of change in different pore types was calculated, as shown in Fig. 8, to demonstrate the effect of LN_2 treatment on the coal pore structure more directly. Five repeated experiments were conducted for dry and wet specimens under one and seven LN_2 treatment cycles, respectively. It can be observed from Fig. 8a~d that the evolution of microporosity, macroporosity and total porosity had a similar trend among repeated experiments, except D-N1-2 and W-N1-2. Although the quantitative alteration of these porosities was distinct. It was noteworthy that mesoporosity might have more complicated evolution trend than other porosities. Because it was easily affected by the increase of microporosity and decrease of microporosity. For wet coal specimens, the effect of cyclic LN_2 treatment on the variation in microporosity was insignificant. The total porosity demonstrated a variation trend similar to microporosity. This could be attributed to the fact that microporosity accounted for more than 90% of the total porosity in the coal specimens. In contrast, macroporosity significantly increased with an increase in the number of LN_2 treatment cycles. In W-N7-1 experiments, the increase of macroporosity exceeded 300%. The average increase of macroporosity after seven LN_2 treatment were over 100%. The difference in variations between micro-, meso-, and macroporosity under cyclic LN_2 treatment might be attributed to the local frost heaving and water migration during water freezing and thawing, which will be detailed in Sect. 4.

Figure 8a, b and f illustrate the variation in the pore structures of the dry coal specimens. It can be observed that the increase in all pore types is insignificant. The variation in the microporosity for dry coal specimens was even lower to that for wet coal specimens and only increased by approximately 3%.

On the other hand, the variance in meso- and macroporosity of dry coal specimens was significantly different from that of wet coal specimens. In some cases, the porosity decreased by more than 60%. This phenomenon highlights the significance of water content in the enhancement of meso- and macroporosity for the cyclic LN_2 treatment of coal. More details are provided in Sect. 4.

3.4 SEM observation

Several fractures were identified on the coal specimen surface for SEM examination to determine the effect of the LN_2 treatment on fracture propagation. Figure 9 illustrates the SEM images of these fractures. It can be observed from Fig. 9a that the aperture of fracture 1 increased from 4.93 to 5.12 μm, while the fracture 2 propagated to the margin of the SEM image. In Fig. 9b, fracture 3 spread to form a "Y" shape fracture after coal impact treatment. The SEM observations verified that the coal impact treatment could lead to changes in the coal fracture structure and increase macroporosity, which is critical for enhancement of coal permeability.

4 Discussion

4.1 Relationship between experimental results

Although the coal properties were investigated using different devices, we obtained unanimous experimental results that demonstrated the effects of cyclic LN_2 treatment on coal specimens. The experimental results are shown in three types: mechanical properties, permeability, and pore size distribution. The mechanical properties of coal depend on the initiation and propagation of micro-fractures and flaws, which can be reflected in the variation of pore structures. Macropores and fractures are the flow channels of coal for fluids that control the coal permeability. As a consequence, the three different sorts of experimental findings were interconnected and could be used to corroborate one another.

The primary analytical agreement in this study was based on the experimental NMR data. Therefore, five repeated experiments for dry and wet coal specimens under 1 and 7 LN_2 treatment cycles were conducted to certify the experimental results. The wide
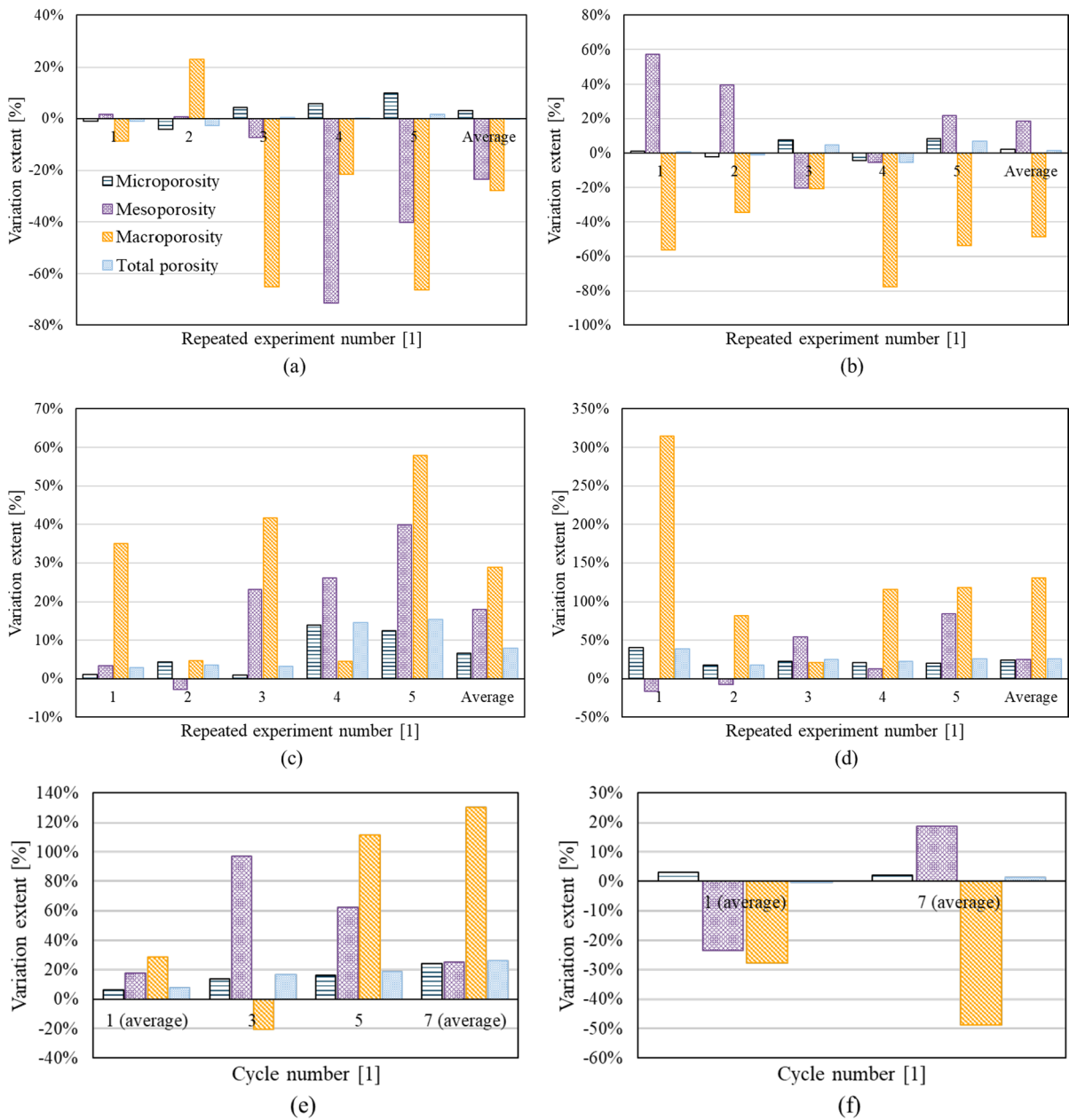
Fig. 8 Quantitative variation in pore structure for different coal specimens under different LN$_2$ treatment cycles: **a** repeated experiments of dry specimens after one LN$_2$ treatment cycle (D-N1-1, 2, 3, 4, 5); **b** repeated experiments of dry specimens after seven LN$_2$ treatment cycle (D-N7-1, 2, 3, 4, 5); **c** repeated experiments of wet specimens after one LN$_2$ treatment cycle (W-N1-1, 2, 3, 4, 5); **d** repeated experiments of wet specimens after seven LN$_2$ treatment cycle (W-N7-1, 2, 3, 4, 5); **e** wet specimens after 1~7 cycles; (f) dry specimens after 1~7 cycles

pore size distribution demonstrated the variation in the pore structures of coal from the nanometer to the millimeter scale before and after the cyclic LN$_2$ treatment. For wet coal specimens, combining NMR and nano-indentation, we found that their results (Fig. 10) consistently indicated the lower effects of cyclic LN$_2$ treatment on coal specimens at the microscale. As can be seen from Fig. 10, there is a strong correlation
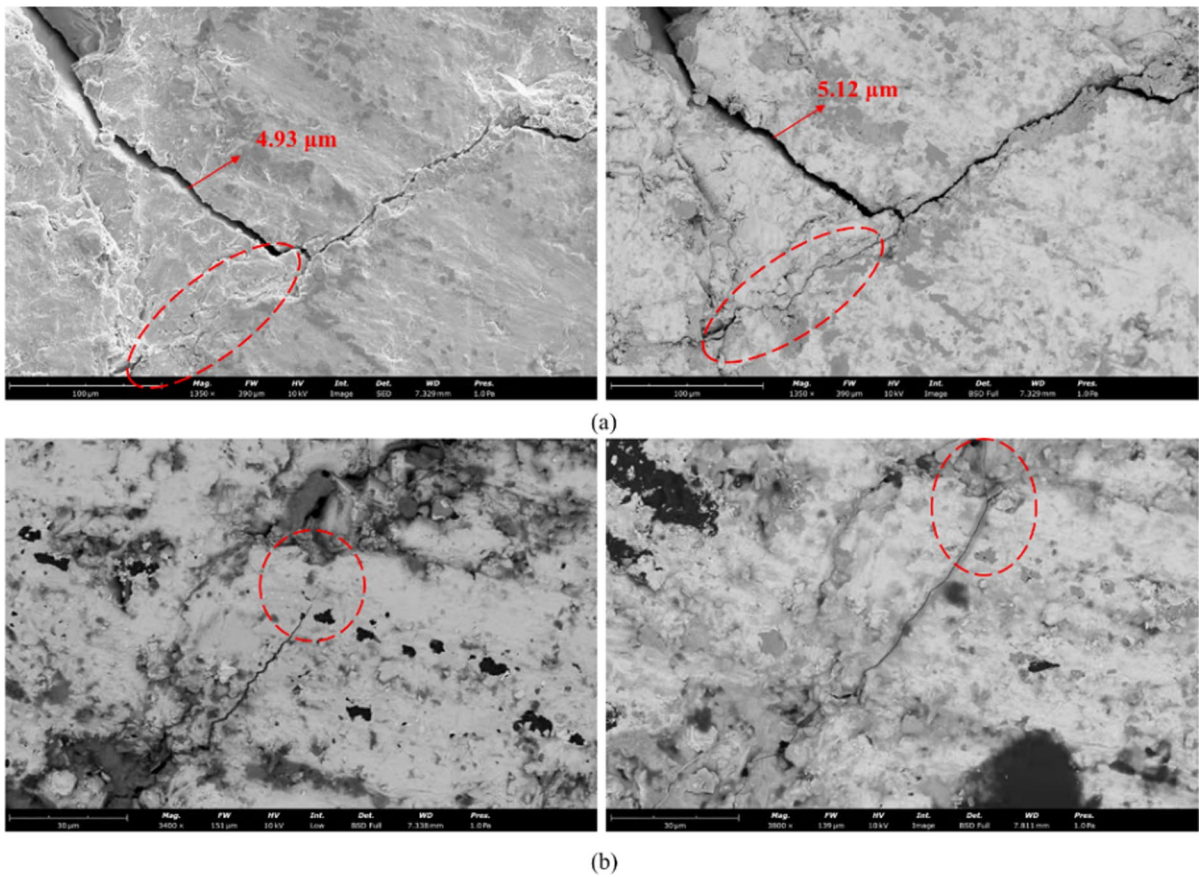
Fig. 9 SEM images of microfracture opening and propagation before and after LN$_2$ treatment: **a** Observation area A; **b** Observation area B
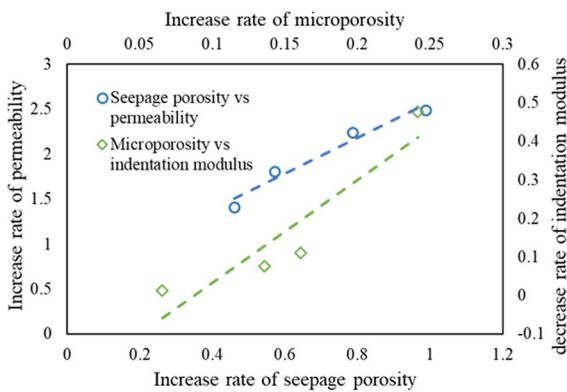
Fig. 10 Correlation between NRM and permeability/indentation results

between the changes in the micropores and the changes in the micromechanical properties. Although the micropores and micromechanical properties were changed after liquid nitrogen treatment. However, the variation in micropores and micro-mechanical properties was insignificant until the seventh cycle of LN$_2$ treatment. After that, the micropores and micro-mechanical properties of the coal specimens increased significantly and then declined. This phenomenon also indicated that the micro-properties and structures were not sensitive to cyclic impact. In contrast, the increase in permeability and macro-porosity (Fig. 10) unanimously demonstrated the significant effects of LN$_2$ treatment on coal fracture systems.

Permeability and macroscopic porosity were strongly correlated, and both changed significantly after liquid nitrogen treatment, and the trends were positively proportional to the cycling time of the LN2 treatment. Recently, similar results were uncovered by Qin et al. (2023) through the investigation of unfrozen water and heat transfer during LN_2 treatment.

For dry coal specimens, only NRM was used to investigate the variation in pore structures before and after cyclic LN_2 treatment because it was found that the effect of LN_2 treatment on coal porosity was insignificant even after multiple LN_2 treatment cycles. However, the variation in the pore size distribution revealed that micro- and macro-pore responded differently to the LN_2 treatment. It was illustrated in Fig. 8 that the macro-porosity of almost every dry coal specimen underwent a substantial decrease, except for D-N1-2 (total porosity decreased 2.67%). The evolution of meso-porosity fluctuated among dry coal specimens. This could be attributed to the fact that, after cyclic LN_2 treatment, some macropores converted to mesopores. It complicated the investigation of the variation in the original meso-pores. However, the variation in micro-porosity was negligible compared to the decrease in macro-porosity after cyclic LN_2 treatment.

Generally, the variation in global porosity and permeability of coal specimens after the cyclic LN_2 treatment demonstrated a similar evolution tendency compared to the previous studies. However, we found that the variation in the pore structures from the micro- to the macroscale of dry and wet specimens responded differently to cyclic LN_2 treatment. Moreover, opposite evolution tendencies of pore structures at the different scales were observed in the same coal specimen. This implies that the impact mechanisms of cyclic LN_2 treatment on micro- and macropores are distinct and have not been comprehensively discussed before.

4.2 Thermal stress and freezing contraction

The volume expansion or contraction induced by the change in temperature is a basic physical phenomenon for solids. However, the extent of variation in the volume of different substances has different responses to temperature change, which is regarded as the thermal expansion coefficient. Coal is a typical composite consisting of minerals and organic compounds. Due

Table 3 Mineral content and corresponding thermal expansion coefficients (Kim et al. 2014)

Minerals	Content (%)	Thermal expansion coefficient (10^{-6}/°C)
Quartz	5.7	11 ~ 16.6
Calcite	14.6	6.7
Pyrite	16.6	8.66
Clay	63.1	9.5 ~ 11.0
Organics	\	35 ~ 50

to the different thermal expansion coefficients of its components, inconsistent thermal deformation may result in compressive or tensile stress between the different components. It is regarded as a heterogeneous thermal stress that occurs widely in composites. Either an increase or decrease in temperature enables the induction of thermal stress in coal specimens. Table 3 presents the mineral components of the experimental coal and their corresponding thermal expansion coefficients. Minerals usually fill or intrude into coal organics as particles or bands, as illustrated in Fig. 11. Therefore, inconsistent thermal deformation could induce thermal expansion stress on minerals and organics, which can be calculated by the following equations.

$$\Delta\sigma_t = \Delta\alpha_{o-m}\Delta T E_o \delta_{ij} \tag{9}$$

where $\Delta\alpha_{o\text{-}m}$ is the difference between the thermal expansion coefficients of minerals and organics. ΔT is the temperature variation. E_o is the elastic modulus of the coal organics, which can be obtained for the indentation experiments (5.5 GPa). Because the thermal expansion coefficients of the minerals in coal are close to each other, they differ dramatically from those of organics. Only the thermal expansion stress between minerals and organics was calculated.

Considering that the temperature variation ΔT during LN_2 treatment was 225 °C (room temperature of 25 °C to LN_2 temperature of −200 °C), the difference in the thermal expansion coefficient between the minerals and organics $\Delta\alpha_o$ ranges from 18.4–43.3, inducing a thermal stress of 22.8–53.6 MPa. This exceeds the tensile strength of coal organics and may damage the coal. Therefore, several fractures were found near the organic and mineral boundaries. However, most of the mineral sizes in the coal organics were below
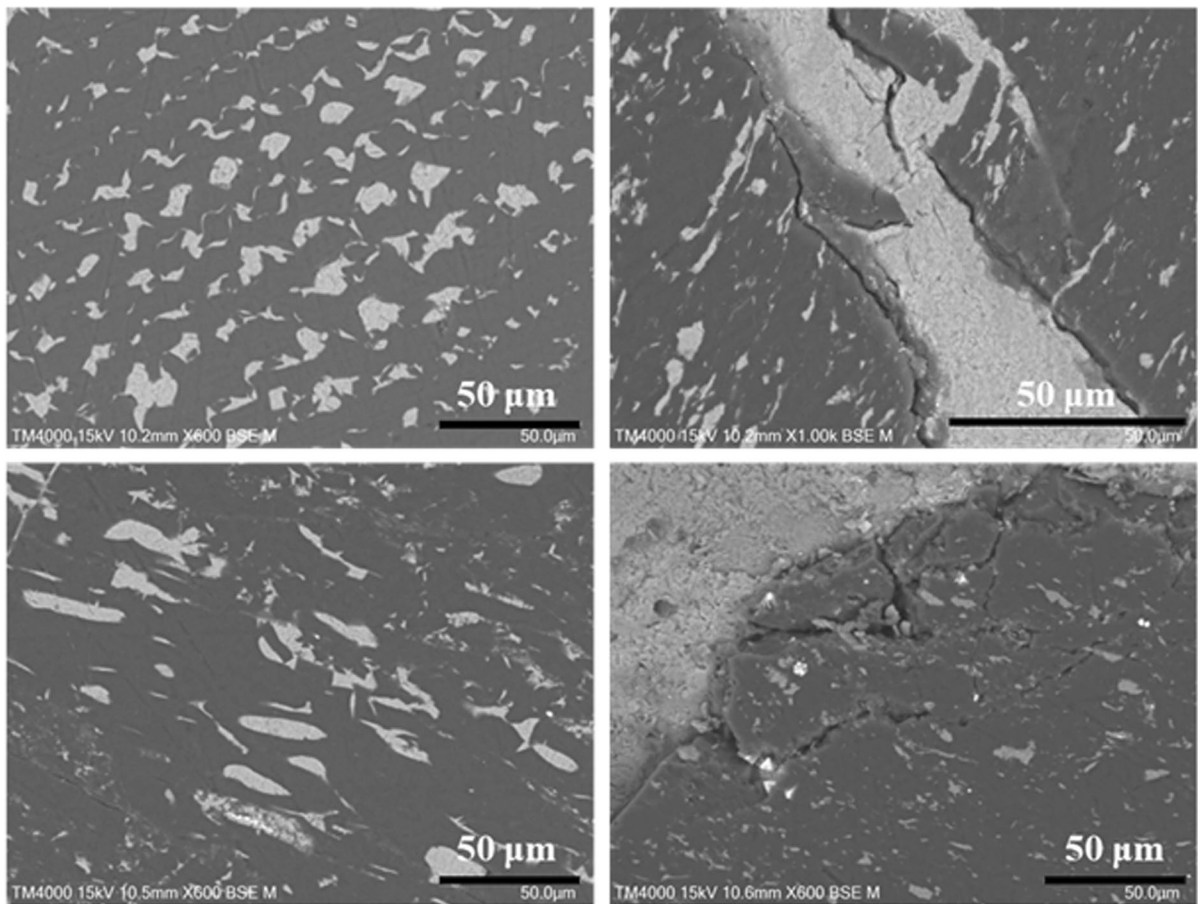
Fig. 11 Mineral particles and bands filling or intruding in coal organics (particle and band size are usually less than 100 μm), white areas represent minerals, black areas represent coal organics, several fractures are around the boundary between organics and minerals

100 μm (Fig. 11). This led to a thermal expansion deformation of less than 1 μm (considering that the thermal expansion strain was less than 9.73×10^{-3}). Therefore, the effect of heterogeneous thermal expansion on coal mainly occurred at the microscale and varied significantly in terms of nano-indentation results and microporosity.

Another effect on the pore structure of coal specimens directly induced by temperature was freezing contraction. During LN_2 treatment, owing to the relatively weak mechanical properties of the coal pore and fracture system (Azarafza et al. 2017), the contraction of the coal skeleton had the tendency to invade the void space and compress pores and fractures. The compression of pores and fractures during coal freezing might accumulate plastic

deformation, which was not able to recover after the LN_2 treatment. The accumulative plastic deformation resulted in the shrinkage and closure of pores and fractures. However, the thermal stress could induce the increase of micropores in coal matrices, which could offset the shrinkage of micropores. Therefore, due to the participation of thermal stress, the decrease in the microporosity of dry specimens was less significant than that in the mesoporosity and macroporosity (seepage pores) in dry specimens. In addition, our previous study (Jiang et al. 2021) indicated that the permeability of coal specimens decreases with an increase in loading and unloading cycles. The above analysis implied that the cyclic LN_2 treatment may cause damage to the permeability of coal seams without the presence

of pore and fracture water. However, evidently, the above analysis did not apply to the wet coal specimens, wherein frost heaving dominated the variation in the physical properties.

4.3 Frost heaving induced by water/ice phase transition

Frost heaving was initially concerned with and extensively researched in the field of freezing soil. The inhomogeneous deformation of freezing soil causes damage to roads, foundations, and other infrastructure in frozen areas. The primary reason for soil deformation is the 9% volume expansion from water to ice during the phase transition (Huang et al. 2018). However, the icing process in porous media is more complicated compared to that exposed in the air. Although numerous studies have investigated the frost heaving in soil and rocks, many issues such as ice segregation, premelted water films, and its stress state remain unresolved in terms of experiments or theoretical analysis. Moreover, the freeze and thawing in coal specimens induced by the LN_2 treatment is different from that in natural soil and rocks induced by weathering, especially in terms of freezing rate and time. In the next section, in-situ frost heaving and water migration in wet coal specimens during cyclic LN_2 treatment will be discussed.

4.3.1 In-situ frost heaving

Previous studies on LN_2 treatment in coal specimens demonstrated substantially different results between the dry and wet specimens. The difference in results was attributed to the effects of frost heave force on macroscopic mechanical properties, coal permeability, and porosity. The majority of studies take into account the frost heave force during in-situ frost heaving. It regards pores and fractures in coal as confined spaces that do not allow unfrozen water to migrate from pores and fractures to other spaces. Under this condition, the pressure of unfrozen coal will eventually equalize with the ice pressure. The frost heavy force is extremely high, and ice pressure can reach 13.7 MPa/°C (ice pressure can surpass 2700 MPa for LN_2 treatment at a fully saturated pore or fracture, which greatly exceeds the tensile strength of coal). However, when the pore or fracture is not

fully saturated, the ice pressure rapidly decreases. As a result, frost-heavy forces were thought to cause severe damage when the water saturation of porous media exceeded 91% (Hirschwald 1908). However, the water saturation among different pore sizes was not homogeneous. The process of water saturation depends on capillary forces and absorption velocity. Micropores have a higher capillary force but a lower absorption velocity (Hall and Hoff 2021). Therefore, it was difficult for water to fully fill the micropores even after a long time of saturation. However, water could enter the macropores and fractures more easily. The high-water saturation of the macropores and fractures could cause more severe damage to these pores and fractures. Thus, the variation in micro-porosity of wet specimens was not as significant as that in meso- and microporosity.

4.3.2 Effect of water migration

When temperatures drop below freezing, the presence of unfrozen supercooling water and premelted water films (Webber et al. 2007) complicates ice formation in porous media. It was found that ice grows first in the larger pores, while the smaller pores still contain supercooled water (Everett 1961). If pores and fractures are treated as an open system, water can migrate from the original pores and fractures to other spaces. The ice pressure in a pore or fracture can be connected to the unfrozen-water pressure in other pores and fractures through a premelted water film between the ice and the pore/fracture wall (Fig. 12 water migration part). According to primary frost heave (capillary theory), the Young–Laplace equation for the pressure difference across a curved ice–water interface can be expressed as (Peppin and Style 2013):

$$P_i - P_w = P_c = \frac{2\gamma_{iw}}{r} \tag{10}$$

P_i is the ice pressure which is the stress applied to pore/fracture walls. γ_{iw} is surface tension between ice and water. r is the radius of the pore/fracture. Considering the ice grows a narrow pore/fracture, the propagation of the pore/fracture may result in the decrease of ice pressure P_i below P_c. The water pressure, P_w,

Fig. 12 Mechanism of local frost heaving and water migration in the coal pores and fractures at different scales
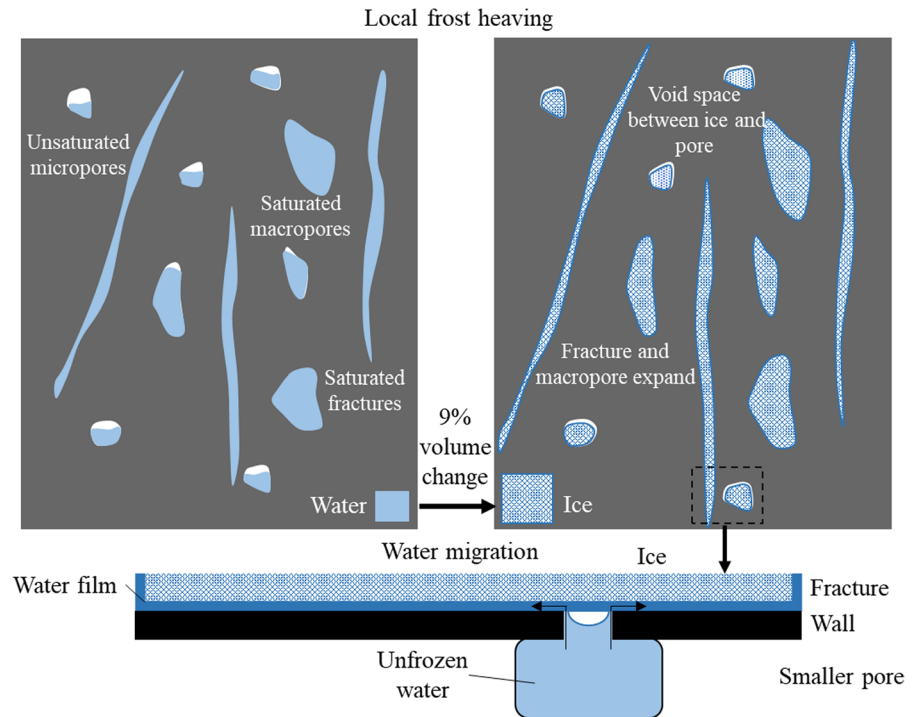
represents suction. Moreover, the increase of moisture in coal can reduce the mechanical properties of coal fractures which may result in the decrease of fracture tensile and shear strength. Therefore, the ice growth in larger pores might attract water migration from other smaller pores to the larger pores. It will further decrease the water saturation in the smaller pores, which will reduce the extent of ice expansion and weaken the frost heaving. This might be another reason that resulted in the insignificant increase in microporosity compared to meso- and macroporosity. However, the occurrence of water migration and its extent at the laboratory scale remain to be discussed, since the rapid freezing rate and ultra-low temperature of LN_2 treatment.

4.4 Limitations and field implications

In the previous section, we have comprehensively discussed the different mechanisms of LN_2 treatment on dry and wet coal specimens. The reasons for the inconsistent evolution of the pore structures at the different scales were attributed to the thermal stress and freezing shrink in dry specimens, and original water-saturation difference between micro- and macropores,

and water migration from smaller to larger pores. The above-mentioned analysis on local frost heaving and water migration, on the other hand, assumed that the pore and fracture system was fully confined or opened. In a real situation, due to the rapid freezing rate in LN_2 treatment, the connection of pores and fractures with the external space should alternate between being fully confined and fully opened. The extent of the connection and water migration require further studies.

In the application field, the effects of LN_2 treatment on micropores may encounter a more severe situation because the water in coal seams is originally stored in the fracture system. The gas in the matrix pore system provides space for ice growth without generating ice pressure. Even if injecting extra water into coal seams, it is difficult to increase water saturation in micropores. Moreover, during the field application of the LN_2 treatment, coal seams undergo a slower freezing rate, which provides sufficient time for water to migrate from smaller pores to larger pores. Therefore, the effects of the LN_2 treatment on micropores are required to be further investigated in field applications.

5 Conclusion

In this study, the evolution of the pore structure and mechanical properties at the microscale under cyclic LN_2 treatment was comprehensively studied through nano-indentation experiments, nuclear magnetic resonance experiments, permeability measurements, and scanning electron microscopy observations before and after the LN_2 treatment. The significant difference in the evolution of coal properties at the different scales were observed in either dry or wet specimens. Different mechanisms were proposed and discussed to reveal the effects of cyclic LN_2 treatment on the pore structure at the different. The main conclusions are as follows:

(1) The consistent experimental results from nano-indentation, NMR, and permeability measurements indicated that the pore structures at the different scales responded differently to the cyclic LN_2 treatment, even in the same dry or wet coal specimens. For dry specimens, microporosity increased at an insignificant rate with an average increase of 3% and 2.07% after 1 and 7 LN2 treatments, macroporosity underwent substantial decrease, with an average decrease of 27.71% and 48.63% after 1 and 7 LN2 treatment. For wet specimens, a slightly higher increase rate of microporosity was observed with an average increase of 6.56% and 24.17% after 1 and 7 LN2 treatments, whereas macroporosity significantly increased with an average increase of 28.78% and 130.39% after 1 and 7 LN_2 treatments.

(2) Heterogeneous thermal deformation and freezing shrink were two opposite effects on dry specimens during LN_2 treatment. The significant difference in thermal deformation between organics and minerals in coal matrices could result in the damage near the boundary of organics and minerals. Freezing shrink might cause the contraction of pores and fractures. Without the offset of new and micro- pores and fractures, coal fracturing suffered significant decrease. This implied that LN_2 treatment might be harmful for coal seams without the presence of water in pores and fractures.

(3) The expansion and propagation of pores and fractures in wet coal specimens depended on the process of frost heaving that was mainly controlled by the original water saturation and water migration during LN_2 treatment. Due to the lower water saturation, LN_2 treatment might have less effects on coal micropores than that on macropores and fractures, even under a local frost heaving condition. Considering the connection of unfrozen water, the larger pores or fractures would attract water from the smaller pores that might further weaken the effects of LN_2 treatment on micropores.

Author contribution Changbao Jiang: Conceptualization. Qi Sun: Writing—Original Draft, Supervision. Bozhi Deng: Formal analysis, Data analysis and Writing. Bowen Yang: Methodology. Jianquan Guo: Funding acquisition.

Data availability The data is available, when it is requested.

Declarations

Ethics approval Not applicable.

Consent to publish All authors consent to submit the paper to Geomechanics and Geophysics for Geo-Energy and Geo-Resources.

Competing interests On behalf of all authors, the corresponding author states that there is no conflict of interest.

References

Azarafza M, Feizi-Derakhshi MR, Azarafza M (2017) Computer modeling of crack propagation in concrete retaining walls: a case study. Comput Concr 19(5):509–514

Cai CZ, Li GS, Huang ZW et al (2014) Rock pore structure damage due to freeze during liquid nitrogen fracturing. Arab J Sci Eng 39(12):9249–9257

Cai CZ, Li GS, Huang ZW et al (2015) Experiment of coal damage due to super-cooling with liquid nitrogen. J Nat Gas Sci Eng 22:42–48

Cai CZ, Gao F, Li GS et al (2016) Evaluation of coal damage and cracking characteristics due to liquid nitrogen cooling on the basis of the energy evolution laws. J Nat Gas Sci Eng 29:30–36

Cheng M, Fu X, Chen Z et al (2023) A new approach to evaluate abandoned mine methane resources based on the zoning of the mining-disturbed strata. Energy 274:127307

Everett DH (1961) The thermodynamics of frost damage to poroussolids. Trans Faraday Soc 57:1541–1551

Feng G, Zhang A, Hu S et al (2018) A methodology for determining the methane flow space in abandoned mine gobs and its application in methane drainage. Fuel 227:208–217

Hall C, Hoof WD (2004) Water transport in brick, stone and concrete. Cement Concrete Res 34(11):2169–2169

Han SC, Cheng YF, Gao Q et al (2018) Experimental study of the effect of liquid nitrogen pretreatment on shale fracability. Journal of Natural Gas Science & Engineering 60:11–23

Hirschwald J (1908) Die Prüfung der natürlichen Bausteine auf ihre Wetterfeständigkeit. W. Ernst & Sohn

Hou P, Chen G, Su S et al (2021) Influence of various control factors on fracture toughness and fracture energy of sandstone subjected to liquid nitrogen cooling. Energy Fuels 36(1):397–406

Huang S, Liu Q, Liu Y et al (2018) Frost heaving and frost cracking of elliptical cavities (fractures) in low-permeability rock. Eng Geol 234:1–10

Jiang CB, Wang YF, Duan MK et al (2021) Experimental study on the evolution of pore-fracture structures and mechanism of permeability enhancement in coal under cyclic thermal shock. Fuel 304:121455

Khadijeh M, Yehya A, Maalouf E (2022) Propagation and geometry of multi-stage hydraulic fractures in anisotropic shales. Geomech Geophys Geo-Energy Geo-Resour 8(4):124

Kim K, Kemeny J, Nickerson M (2014) Effect of rapid thermal cooling on mechanical rock properties. Rock Mech Rock Eng 47(6):2005–2019

Li H, Lin BQ, Chen ZW et al (2017) Evolution of coal petrophysical properties under microwave irradiation stimulation for different water saturation conditions. Energy Fuels 31:8852–8864

Li D, Su X, Su L (2021) Theory of gas traps in stope and its application in ground extraction of abandoned mine gas: part 1–gas trap in stope and resources estimation. J Petrol Sci Eng 207:109285

Li Y, Hu W, Wei S et al (2022) Influence of preexisting discontinuities on hydraulic fracture complexity in a naturally fractured reservoir. Eng Geol 311:106919

Liu J, Zhao Y, Tan T et al (2022) Evolution and modeling of mine water inflow and hazard characteristics in southern coalfields of China: a case of Meitanba mine. Int J Min Sci Technol 32(3):513–524

Momeni A, Abdilor Y, Khanlari GR et al (2016) The effect of freeze–thaw cycles on physical and mechanical properties of granitoid hard rocks. Bull Eng Geol Environ 75:1649–1656

Ottiger S, Pini R, Storti G et al (2008) Measuring and modeling the competitive adsorption of CO_2, CH_4, and N_2 on a dry coal. Langmuir 24(17):9531–9540

Peppin SSL, Style RW (2013) The physics of frost heave and ice-lens growth. Vadose Zone J. https://doi.org/10.2136/vzj2012.0049

Ping L, Lai Z, Sen C et al (2020) Main challenges of closed/abandoned coal mine resource utilization in China. Energy Sour Part A Recovery Util Environ Effects 42(22):2822–2830

Qin L, Zhai C, Liu S et al (2016) Failure mechanism of coal after cryogenic freezing with cyclic liquid nitrogen and its influences on coalbed methane exploitation. Energy Fuels 30(10):8567–8578

Qin L, Zhai C, Liu SM et al (2017) Changes in the petrophysical properties of coal subjected to liquid nitrogen freeze-thaw – a nuclear magnetic resonance investigation. Fuel 194:102–114

Qin L, Zhai C, Xu JZ et al (2019) Evolution of the pore structure in coal subjected to freeze−thaw using liquid nitrogen to enhance coalbed methane extraction. J Petrol Sci Eng 175:129–139

Qin L, Ma C, Li S et al (2022) Liquid nitrogen's effect on the mechanical properties of dried and water-saturated frozen coal. Energy Fuels 36(4):1894–1903

Qin L, Lin S, Lin H et al (2023) Distribution of unfrozen water and heat transfer mechanism during thawing of liquid nitrogen immersed coal. Energy 263:125905

Stoss K, Valk J (1979) Uses and limitations of ground freezing with liquid nitrogen. Developments in geotechnical engineering. Eng Geol 13:485–494

Su SJ, Gao F, Cai CZ et al (2020) Effect of low temperature damage on tensile strength of coal under the liquid nitrogen freezing. Therm Sci 24(6 Part B):3979–3986

Sun Y, Zhao Y, Li Y et al (2023) Impact of liquid nitrogen freeze–thaw on multistage gas flow: differences between shallow and deep coal in Qinshui Basin. Geomech Geophys Geo-Energy Geo-Resour 9(1):41

Wang YQ, Dai MH, Liu K et al (2020) Research on surface heat transfer mechanism of liquid nitrogen jet cooling in cryogenic machining. Appl Therm Eng 179:115607

Webber JBW, Dore JC, Strange JH et al (2007) Plastic ice in confined geometry: the evidence from neutron diffraction and NMR relaxation. J Phys Condens Matter 19(41):415117

Wolkersdorfer C, Walter S, Mugova E (2022) Perceptions on mine water and mine flooding–an example from

abandoned West German hard coal mining regions. Resour Policy 79:103035

Won J, Lee D, Choi HJ et al (2022) Field experiments for three freezing operation scenarios in silty soil deposits. Eng Geol 303:106642

Xie HP, Gao MZ, Gao F et al (2017) Strategic conceptualization and key technology for the transformation and upgrading of shut-down coal mines. J China Coal Soc 42(6):1355–1365

Yin G, Shang D, Li M et al (2018) Permeability evolution and mesoscopic cracking behaviors of liquid nitrogen cryogenic freeze fracturing in low permeable and heterogeneous coal. Powder Technol 325:234–246

Yuan L, Jiang YD, Wang K, Zhao YX et al (2018) Precision exploitation and utilization of closed/abandoned mine resources in China. J China Coal Soc 43(1):14–20

Zhai C, Qin L, Liu S et al (2016) Pore structure in coal: pore evolution after cryogenic freezing with cyclic liquid nitrogen injection and its implication on coalbed methane extraction. Energy Fuels 30(7):6009–6020

Zhang LF, Hascakir B (2021) A review of issues, characteristics, and management for wastewater due to hydraulic fracturing in the U.S. J Pet Sci Eng 202:108536

Zhang P, Liang X, Xian C et al (2022) Geomechanics simulation of stress regime change in hydraulic fracturing: a case study. Geomech Geophys Geo-Energy Geo-Resour 8(2):83

Zoback MD, Healy JH, Roller JC (1977) Preliminary stress measurements in central California using the hydraulic fracturing technique. Pure Appl Geophys 115(1):135–152